Applied Geochemistry 130 (2021) 104994

Contents lists available at ScienceDirect

Applied Geochemistry

journal homepage: www.elsevier.com/locate/apgeochem

Detection of the multivariate geochemical anomalies associated with mineralization using a deep convolutional neural network and a pixel-pair feature method

Chunjie Zhang, Renguang Zuo *, Yihui Xiong

State Key Laboratory of Geological Processes and Mineral Resources, China University of Geosciences, Wuhan, 430074, China

ARTICLE INFO

Editorial handling by Dr. Z Zimeng Wang

Keywords:
Geochemical anomalies
Mineral exploration
Pixel-pair feature method
Deep learning
Convolutional neural network

ABSTRACT

Machine learning (ML) algorithms are widely applied in various fields owing to their strong ability to abstract high-level features from a large number of training samples. However, few supervised ML algorithms have been applied in geochemical prospecting and mineral exploration because mineralization is a rare geological event that leads to an insufficient number of training samples. Generating a large number of training samples is crucial for the application of supervised ML in geochemical prospecting and mineral exploration. In this study, a novel anomaly detection framework combined with a pixel-pair feature (PPF) method and a deep convolutional neural network (CNN) was employed to identify the multivariate geochemical anomalies associated with mineralization. First, the PPF method was employed to generate sufficient training samples by recombining the pixel pairs of the labeled samples. Then, a multilayer supervised CNN framework, which consists of 13 convolutional layers, an average pooling layer, and a fully connected layer, was trained with these pixel pairs for geochemical anomaly recognition. The testing procedure was based on the fact that neighboring pixels belong to the same class with a high probability. The dual-window detector was applied to detect multivariate geochemical anomalies related to Fe polymetallic mineralization in the southwest Fujian Province of China. The identified geochemical anomalies exhibited a close spatial correlation with the known mineral deposits, which validates the potential of the proposed method. Therefore, the method developed in this study can enhance the application of supervised ML in geochemical prospecting and mineral exploration.

1. Introduction

Machine learning (ML) algorithms have shown immense potential in geosciences owing to their strong ability to recognize patterns and insights within vast amounts of Earth system data (Reichstein et al., 2019). ML algorithms can typically be summarized into two categories: supervised and unsupervised learning (Mohri et al., 2018). Supervised learning algorithms, such as logistic regression (Cox, 1959), support vector machines (Vapnik, 1995), random forest (Breiman, 2001), ensemble learning (Dietterich, 2002), artificial neural networks (Anderson, 1972; Bishop, 1995), deep belief nets (Hinton et al., 2006), and convolutional neural network (CNN) (LeCun et al., 1998), focus on enabling machines to classify objects, issues, or situations based on known/labeled data fed into the machines. In contrast, unsupervised learning algorithms, which aim to identify hidden or potential patterns from the input dataset without labeled examples, have been widely applied in the field of clustering (Scott and Knott, 1974; Bezdek et al., 1984), density estimation (Silverman, 1986), dimensional reduction (Redlich, 1993; Fodor, 2002), and feature extraction (Coates et al., 2011). Compared with traditional data analysis methods, ML algorithms are more robust owing to their strong ability to (i) perform complex prediction tasks without the assumption of data patterns, (ii) create a representation of the relationship between inputs and outputs, and (iii) reveal new and unanticipated patterns, structures, and relationships (LeCun et al., 2015; Bergen et al., 2019).

ML represents a substantial contribution to geoscience development, with ML algorithms applied to the fields of remote sensing, geochemistry, geophysics, climate, and other geological fields to solve the key problems of classification, anomaly detection, regression, and space- or time-dependent state prediction (e.g., Ziaii et al., 2009; Cracknell and Reading, 2013; Zhu et al., 2018; Zuo and Xiong, 2018). In the field of geochemical prospecting and mineral exploration, an important step is

* Corresponding author.
E-mail address: zrguang@cug.edu.cn (R. Zuo).

https://doi.org/10.1016/j.apgeochem.2021.104994
Received 3 November 2020; Received in revised form 4 March 2021; Accepted 8 May 2021
Available online 19 May 2021

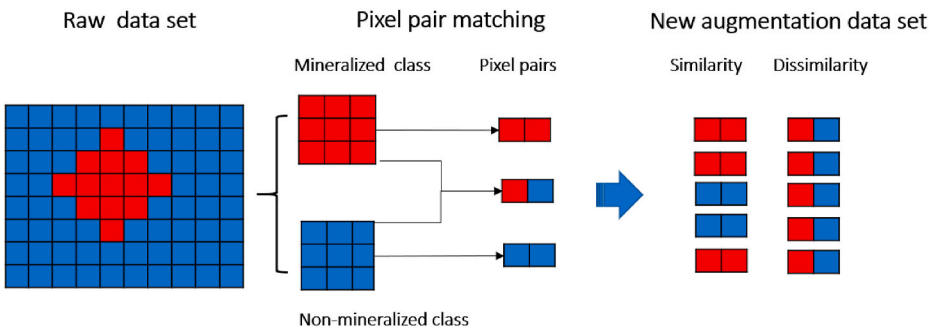

Fig. 1. A diagram showing the principle of PPF.

integrating a conceptual mineral deposit model with available data to support exploration targeting (Yousefi et al., 2019). ML algorithms can obtain valuable information from geoscience data, and have been employed for mineral prospectivity mapping and geochemical anomaly identification (e.g., Kirkwood et al., 2016; Xiong and Zuo, 2016; Zuo et al., 2019; Luo et al., 2020). However, there are still several challenges in the application of ML algorithms in geosciences; for example, rare events that occur infrequently but have great significance to society and the Earth system. Various fields of geosciences include such rare events (Karpatne et al., 2018), such as extreme weather events (e.g., cyclones, flash floods, and heat waves), natural hazards (e.g., landslides, earthquakes, and tornadoes), and impacts to the Earth's biosphere (e.g., deforestation, insect damage, and forest fires). Rare events are characterized by an inadequate number of rare classes (positive samples) and the absence of other classes (negative samples) (Guo et al., 2016; Karpatne et al., 2018), which hinders the development of supervised ML algorithms in these fields. These issues also hinder the application of ML algorithms to geochemical prospecting and mineral exploration.

Over the past several decades, geochemical anomalies have played an increasingly important role in the field of mineral exploration (Cohen et al., 2010; Grunsky, 2010; Zuo and Wang, 2016). ML algorithms have been successfully adopted to identify hidden and unknown geochemical patterns related to mineralization in a complex geological setting (Ziaii et al., 2009, 2012; Gonbadi et al., 2015; Xiong and Zuo, 2016; Chen and Wu, 2017; Zuo, 2017; Zuo and Xiong, 2018, 2020; Luo et al., 2020). These ML algorithms have a strong ability to deal with complex, high-level, and non-linear multivariate geochemical patterns in support of geochemical prospecting and mineral exploration. Supervised learning methods, such as neural networks (Ziaii et al., 2009, 2012; Yu et al., 2019), metric learning (Wang et al., 2019a, 2019b), and support vector machines (Gonbadi et al., 2015), were built with labeled geochemical background and anomaly to produce a probability map that differentiates geochemical anomalies from the background. The delineated geochemical anomalies identified by the supervised ML algorithms exhibited a strong spatial correlation with the locations of known mineral deposits, thereby indicating that supervised ML algorithms can be used as an effective method to identify the geochemical anomalies associated with mineralization (Zuo, 2017; Wang et al., 2019a, 2019b; Li et al., 2020). The supervised learning methods critically rely on training with labeled samples. Usually, the training dataset consists of two types of geochemical patterns, namely, background and anomaly, which can be trained using various supervised ML methods to map geochemical anomalies (Gonbadi et al., 2015). Therefore, the aim of supervised ML algorithms is to recognize the mineralization of interest and to discriminate them from geochemical background (Singer and Kouda, 2001). Though the size and shape of the mineralization cannot be definitively determined, the areas containing known mineral deposits should be anomalous because most magmatic-hydrothermal mineral deposits are surrounded by geochemical halos containing anomalous concentrations of mineralization-related elements that forms because of dispersion within the adjacent soil, sedimentary material, and rocks (Hagemann et al., 2016). Therefore, the areas containing known mineral deposits were usually defined as the labeled anomaly samples. Meanwhile, the background samples were randomly selected from the areas without known mineral deposits (Wang et al., 2019a, 2019b; Li et al., 2020, 2021).

However, mineralization is a rare geological event in nature (Cheng, 2007, 2012), which produces insufficient training samples. Therefore, creating a large number of training samples is challenging in the application of supervised ML to geochemical prospecting and other fields in geosciences (Zuo, 2020). Several studies have addressed the issue of insufficient training samples. For example, Wang et al. (2020) applied semi-supervised learning, which exploits the huge amount of unlabeled data to benefit supervised learning tasks and provide a suitable scheme for mineral prospectivity mapping. Li et al. (2020) adopted transfer learning to overcome a shortage of training samples and extracted the spatial distribution characteristics of a manganese deposit via the AlexNet architecture (Krizhevsky et al., 2012). Furthermore, Li et al. (2021) adopted the data augmentation technique based on a random drop to overcome the sparse number of training samples while using a deep CNN for mineral prospectivity mapping.

In this study, a novel pixel-pair feature (PPF) method is introduced to increase the number of training samples. A CNN adopts deep convolutional layers whose kernels can effectively extract spatial structures features. As an unsupervised CNN methods, a convolutional autoencoder has been successfully used to capture the spatial structure features of the geochemical samples by considering their spatial patterns and local spatial structure, thereby enabling the recognition of multivariate geochemical anomalies via reconstruction errors (Chen et al., 2019; Xiong and Zuo, 2021). Thus, a CNN is capable of capturing the spatial structure features of geochemical patterns. Therefore, a deep CNN framework based on these training samples will be built to detect the multivariate geochemical anomalies associated with Fe polymetallic mineralization in the southwest Fujian Province of China. The main objective of this study is to provide an alternative method of producing sufficient training samples for the application of supervised ML algorithms to geoscience. Furthermore, this study demonstrates the usefulness of deep learning algorithms in geochemical prospecting and mineral exploration.

2. Methods

2.1. Pixel-pair feature model

The PPF method, proposed by Li et al. (2016), was originally designed to increase the number of training samples and guarantee effective training of deep CNN. It was first used for remote sensing image classification and anomaly recognition (Li et al., 2016). The basic idea of PPF is to recombine the pixel pairs of the labeled samples to generate a large sample dataset. The training sample was reconstructed based on the following criteria: (i) if two pixels were selected from the same class, they were marked as "0"; and (ii) if they were selected from different

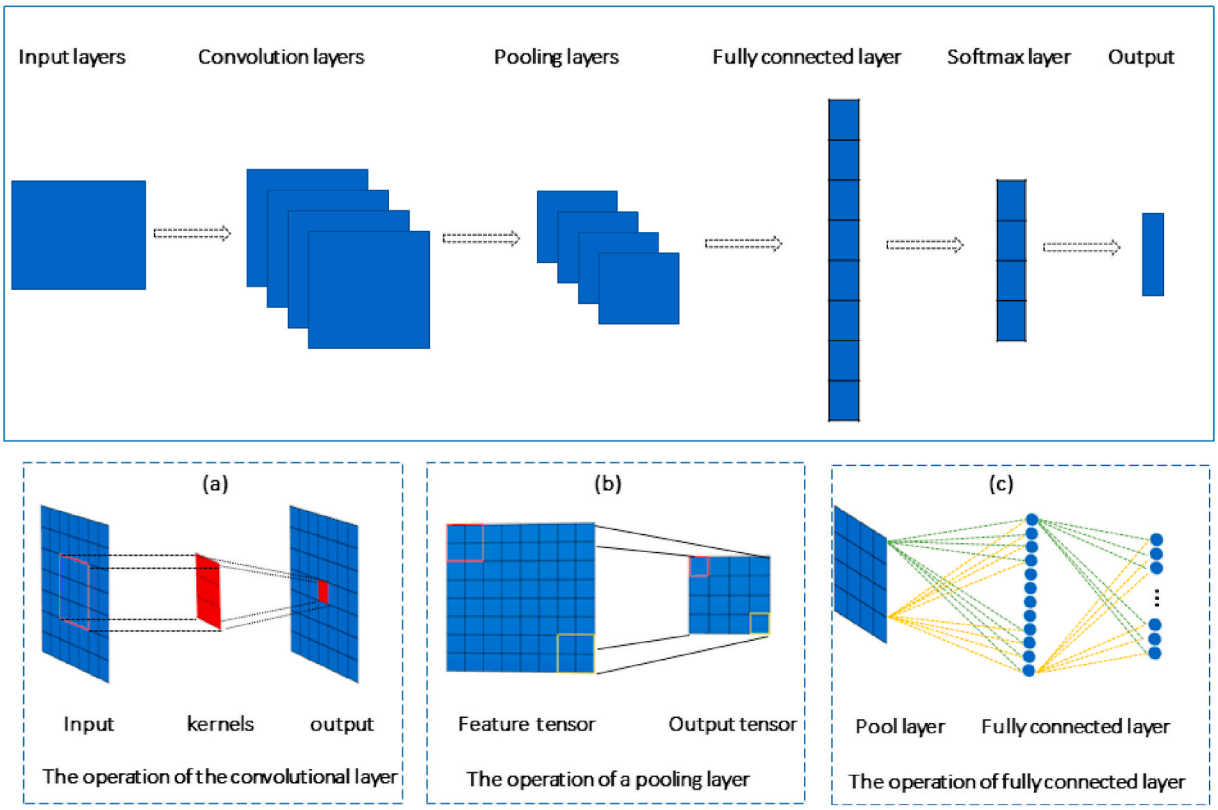

Fig. 2. A common CNN framework.

classes, they were marked as "1". Considering a dataset X with C classes and M labeled samples, the total sample size of X was $M \times C$. After pairing the pixels, the total number of samples labeled "0" which denotes the similarity of two pixels, was calculated as $N = C \times M \times (M-1)$. Suppose $C = 10$ and $M = 100$, N is 99,000, which is much larger than the original number of samples of 1,000 ($C \times M = 10 \times 100$). Meanwhile, the samples labeled "1", which denotes dissimilarity, was M^C (Li et al., 2016).

To identify multivariate geochemical anomalies, a dataset with labeled samples was utilized. The total study area was divided into two classes: mineralized areas (class 1) and non-mineralized areas (class 2). The locations of known mineral deposits and their adjacent areas were considered as mineralized areas (class 1), and the barren areas were regarded as non-mineralized areas (class 2). Suppose that the sample datasets included class 1 areas with N pixels and class 2 areas with K pixels. If the selected two pixels were derived from the same class (class 1 or class 2) (Fig. 1), the two pixels were deemed similar and marked with a new label "0". If the two pixels were derived from different classes, they were deemed dissimilarity and marked as "1". After pixel-pair recombination, the sample size was expanded from $(K + N)$ to $(K \times (K–1) + N \times (N–1) + K \times N)$.

2.2. Convolutional neural network

A CNN is a feedforward neural network that typically contains a convolutional layer, pooling layers, and fully connected layers (Fig. 2). A well-trained CNN can reflect the spatial local correlation by strengthening local connectivity between neurons in adjacent layers (LeCun et al., 1998). The convolutional layers are an important part of CNN for extracting high-level features of input data through a convolutional operation. The convolution layers have three advantages: (i) reducing model parameters via the weight sharing mechanism, (ii) maintaining invariance of the location of the object, and (iii) learning correlations among neighboring pixels via local connectivity (LeCun et al., 1998). A general two-dimensional convolutional operation can be represented by the following calculation formula:

$$G^*(X,Y) = \sum_{i=1}^{m}\sum_{j=1}^{n} f(i,j)\cdot G(x-i+c,\ y-j+c), \quad (1)$$

where $f(x, y)$ is a filter for $n \times m$ dimensional image G, resulting in the central result $G^*(x,y)$ around the central coordinate c. In CNN, each convolution layer learns several filters, f, typically followed by a down-sampling operation in n and m to compress the spatial information, which can serve as a forcing function to learn increasingly complex representations in subsequent convolutional layers (Fig. 2a).

Pooling layers typically interleave with convolutional layers to reduce the dimensions of the output feature maps and network parameters (LeCun et al., 2015). Pooling layers can also keep the translation invariant, similar to convolution layers, because they consider the neighboring pixels. Max pooling and average pooling are two of the most commonly used pooling operations. For 8×8 feature maps, the output maps can be reduced to 4×4 dimensions through a max pooling operator with a 2×2 window size and a two-stride size (Fig. 2b).

Fully connected layers are the last layers of CNN for feature fusion and classification (Krizhevsky et al., 2012). Fig. 2c shows the operation of the fully connected layer, which can flatten the output feature maps into a column vector and then transform the vector into certain categories for classification or employ it as a feature vector for follow-up processing (Guo et al., 2016).

3. Dataset

The study area, located in the southwest of Fujian Province, China, has experienced long-term structural and geological evolution, and has been affected by the Zhenghe-Dapu, Nanping-Ninghua, and Shanghang-Yunxiao faults and their secondary structures. The faults and folds provided favorable spaces and channels for the migration and

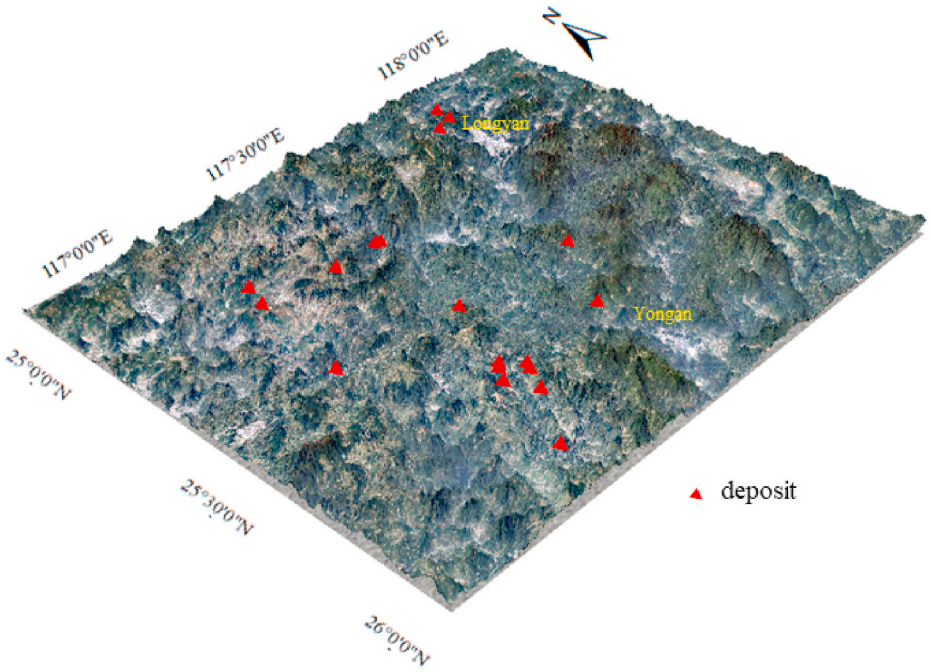

Fig. 3. Maps showing the location of the study area and locations of known mineral deposit (red triangles). (For interpretation of the references to colour in this figure legend, the reader is referred to the Web version of this article.)

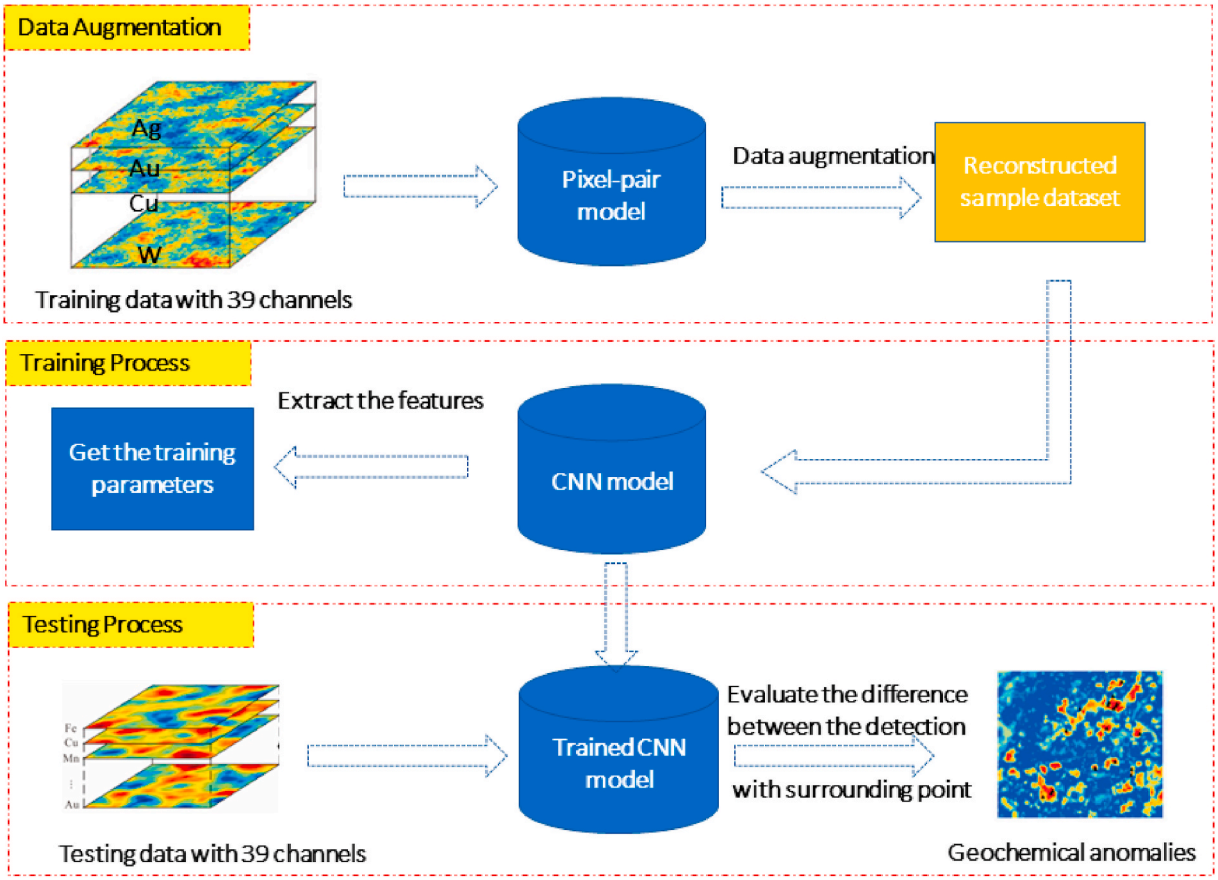

Fig. 4. Experimental framework used in this study.

precipitation of ore-forming hydrothermal fluids. This study area is an important Fe polymetallic metallogenic belt in China (Zhang et al., 2015a, 2015b; Zuo et al., 2015) (Fig. 3). Substantial research has been conducted, revealing several Fe polymetallic deposits in this district, such as the Makeng, Luoyang, Zhongjia, and Pantian Fe deposits (Zhang and Zuo, 2014, 2015; Zhang et al., 2015a, 2015b; Zuo et al., 2015).

Table 1
Number of samples of the original data set, training data, and testing data.

Class	Labeled dataset	Selected dataset	Training dataset	Testing dataset
Class 1 (mineralized areas)	171	171	136	35
Class 2 (non-mineralized areas)	77639	171	136	35
Total number	77810	342	272	70

Table 2
Number of samples in the new dataset after pixel-pair matching.

Label	Training dataset	Testing dataset
0 (similarity)	36720	2380
1 (dissimilarity)	18496	1225
Total number	55216	3605

Further information on the geological setting and mineral deposit model can be found in Zuo et al. (2015) and Zhang et al. (2015a, 2015b).

The geochemical dataset used in this study contained 39 major and trace elements. Xie et al. (1997) described the sampling, analysis, detection limits, and quality control of these geochemical data in detailed. Geochemical exploration data are compositional data that suffer from the data closure problem (Aitchison, 1986); therefore, geochemical data were preprocessed using the isometric logratio transformation to eliminate data closure effects (Egozcue et al., 2003). The dataset used in this study has been extensively explored and validated as a high-quality dataset for inferring the presence of Fe polymetallic mineralization (e.g., Xiong and Zuo, 2016, 2020, 2021; Luo et al., 2020). In this study, the dataset was used to verify whether the PPF and CNN can effectively recognize multivariate geochemical anomalies related to mineralization.

4. Results and discussion

The experimental framework (Fig. 4) can be divided into data augmentation, training, and testing. All programs are implemented based on the Python and Tensorflow library (https://tensorflow. google. cn/).

4.1. Constructing the training dataset

The 39 geochemical elements were first interpolated into grid files with a cell size of 500 m × 500 m using the inverse distance weighted interpolation (Shepard, 1968). Each grid file contains 251 × 310 pixels. The Fe deposit and their surrounding nearest pixels were regarded as mineralized areas. In the experiment, a total of 9 pixels, including Fe deposits and eight surrounding pixels, were regarded as mineralized areas. There were 19 Fe deposits in the study area, resulting in a total of 171 pixels labeled as class 1. Areas not designated as mineralized areas were marked as non-mineralized areas (class 2), containing 77,810 pixels. Therefore, the study area consisted of 171 and 77,810 pixels marked as mineralized (class 1) and non-mineralized areas (class 2), respectively (Table 1). To avoid the influence of unbalanced data for classification and prediction, the same pixel number was randomly selected for non-mineralized areas (171 pixels). 80% of the samples within each individual class were selected as training data, and the remaining samples were used as testing data. Thus, 272 pixels (136 pixels from class 1 and 136 pixels from class 2) were regarded as the training data, and 70 pixels (35 pixels from class 1 and 35 pixels from class 2) were regarded as the testing data (Table 1).

A new set of data containing similar pixel pairs and dissimilar pixel pairs was generated via pixel pair matching. Similar pixel pairs were derived from the same class and marked as "0" whereas dissimilar pixel pairs were derived from different classes and marked as "1" (Table 1). In the training dataset, the samples labeled as "1" contained 18,496 (136 × 136) pixel pairs (dissimilarity) after matching different classes, and the

Table 3
Training results based on 10 randomly selected non-mineralized pixels.

No.	Training Loss	Testing Accuracy
1	0.150	0.878
2	0.197	0.870
3	0.140	0.879
4	0.130	0.848
5	0.097	0.913
6	0.110	0.857
7	0.150	0.892
8	0.106	0.909
9	0.180	0.870
10	0.198	0.877

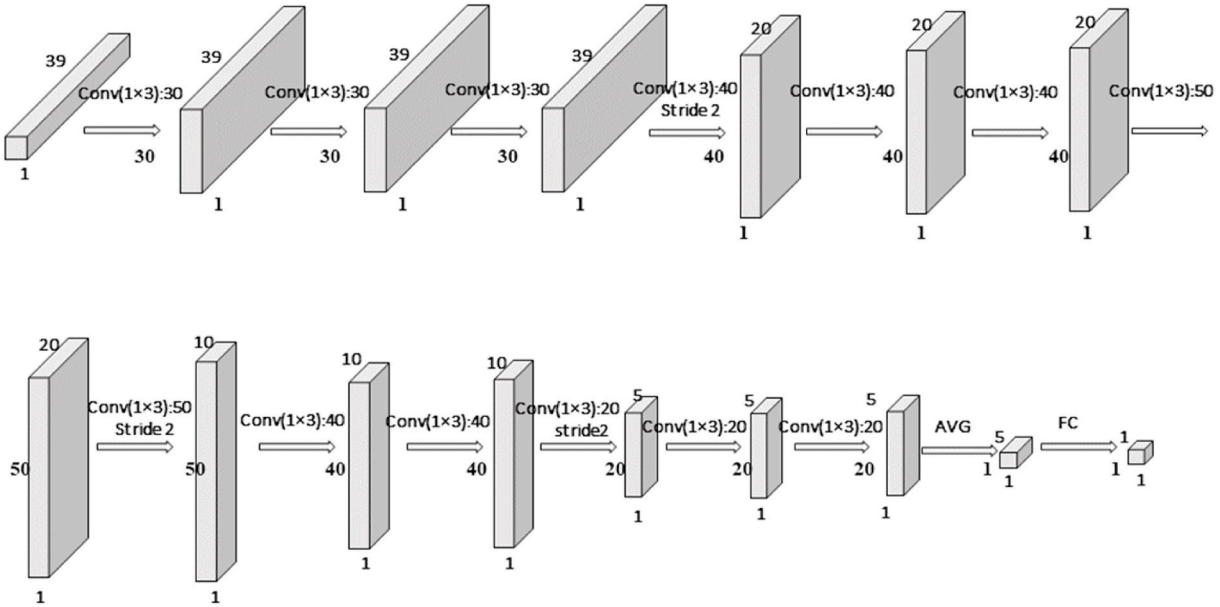

Fig. 5. A diagram showing a CNN framework.

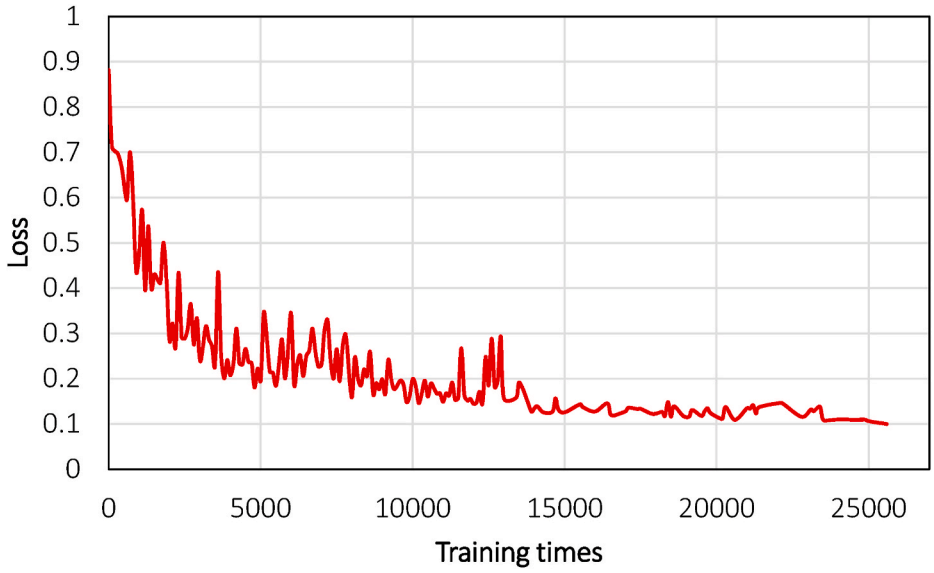

Fig. 6. A plot of loss changes vs. training times.

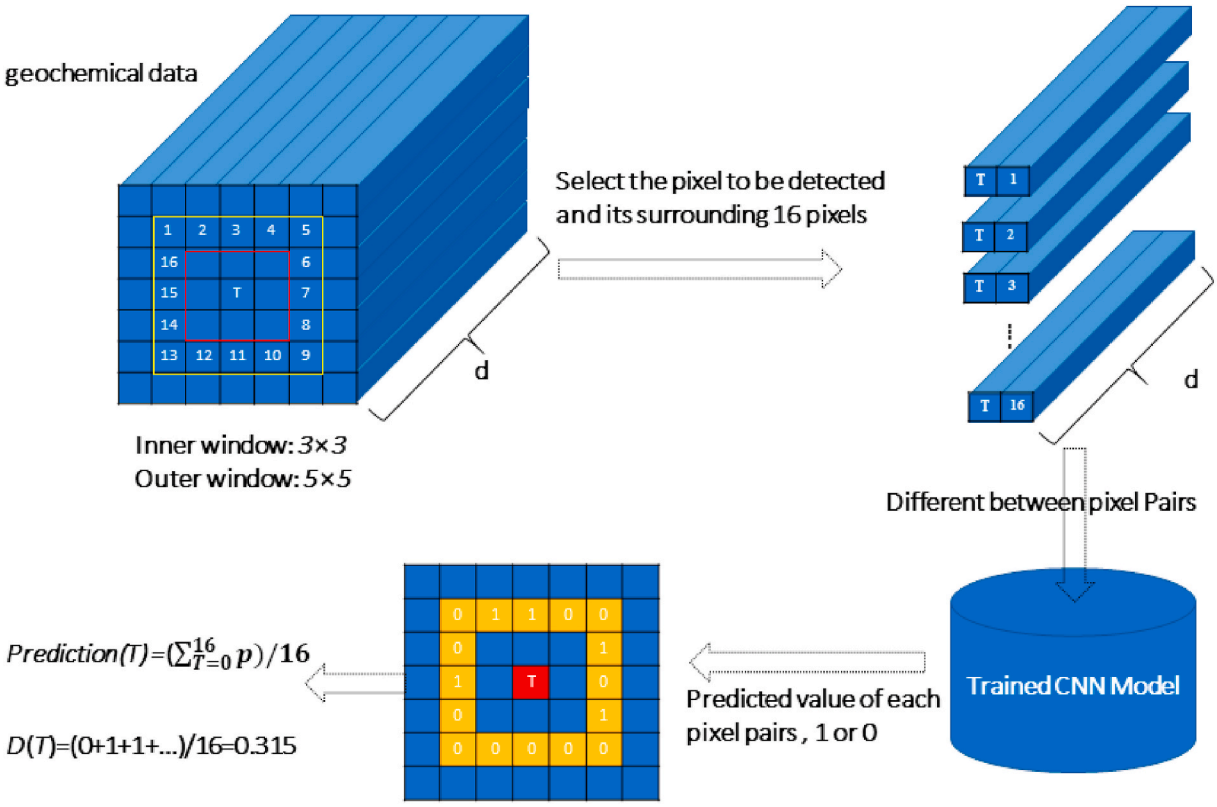

Fig. 7. Pixel pairs based on dual-windows for detecting geochemical anomalies.

samples labeled as "0" (similarity) had 36,720 (2 × 136 × 135) pixels after matching the same class (Table 2). Therefore, after pixel-pair matching, the number of training data increased from 342 to 55,216, and the number of testing data increased from 70 to 3,605 after pixel-pair matching.

4.2. CNN framework

The convolution kernel, convolution layer numbers, and parameters can be adjusted via trial-and-error to extract the features of multivariate geochemical data based on pixel pairs generated by PPF. A deep CNN was built by stacking multiple CNN, which aimed to integrate the low-level features into a higher level of representation (Krizhevsky et al., 2012). This design is powerful for detecting local geometric features, spatial patterns, and larger-scale features in deeper layers. The deep CNN architecture included 13 convolutional layers, an average pooling layer, a fully connected layer, and ReLU layers after each convolutional layer (Fig. 5).

The dimensionality of the input geochemical data was 39. The first convolutional layer (C1) filtered a labeled pixel (1, 39, 1) with 30

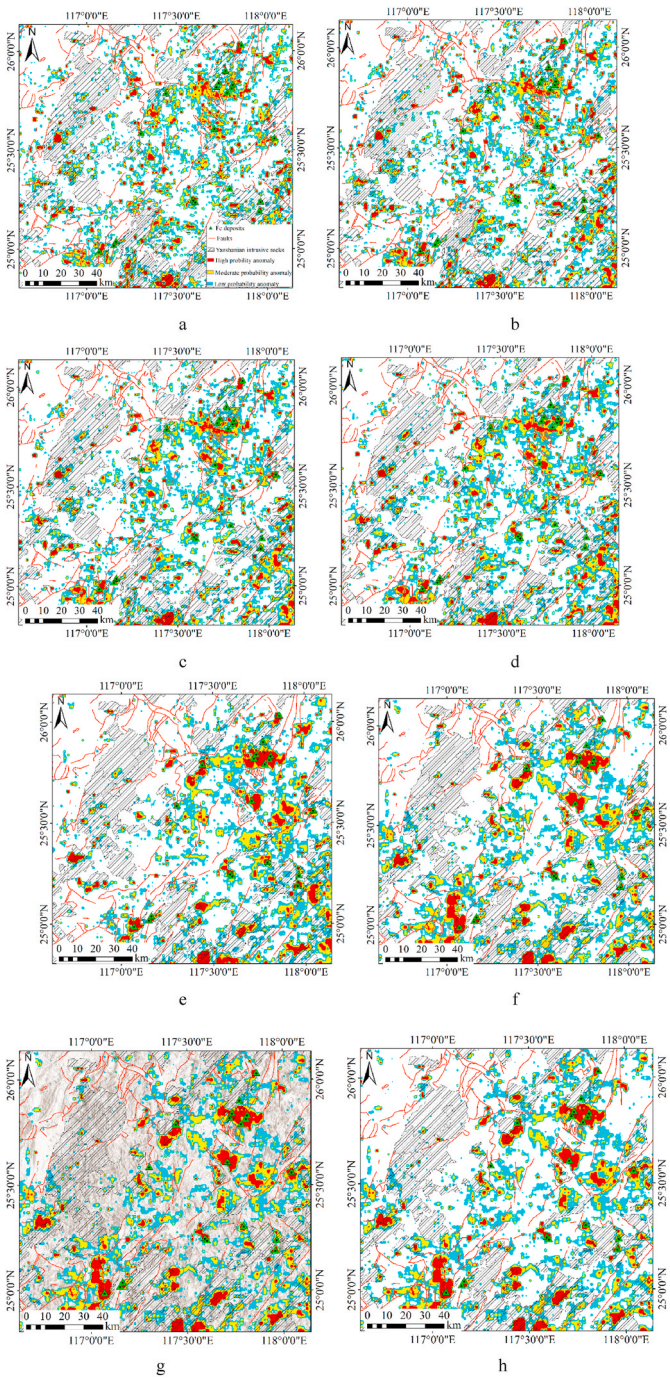

Fig. 8. Identified geochemical anomaly maps with a window size of (a) (5,7), (b) (5,9), (c) (5,11), (d) (5,13); (e) (7,35); (f) (9,35), (g) (11,35); and (h) (13,35).

kernels that had a size of (1, 3, 1), producing a (1, 39, 30) tensor. The second convolution layer (C2) was based on the C1 (1, 39, 30) tensor filters with 30 kernels that had a size of (1, 3, 30), producing a new tensor (1, 39, 30). The third layer (C3) filtered the tensor with 30 kernels that had a size of (1, 3, 30), producing a tensor with the same shape as the C2 layer. The convolutional layers (C4) with a stride of two were used to reduce the dimensionality, and a tensor of (1, 20, 40) was generated. Subsequently, seven convolutional kernels were used to extract and learn the features, and two convolutional layers (C4) with a stride of two were used to reduce the dimensions to the desired value. The C13 tensor was fed into an average pooling layer. Finally, the chain of the CNN architecture ended in a fully connected network for

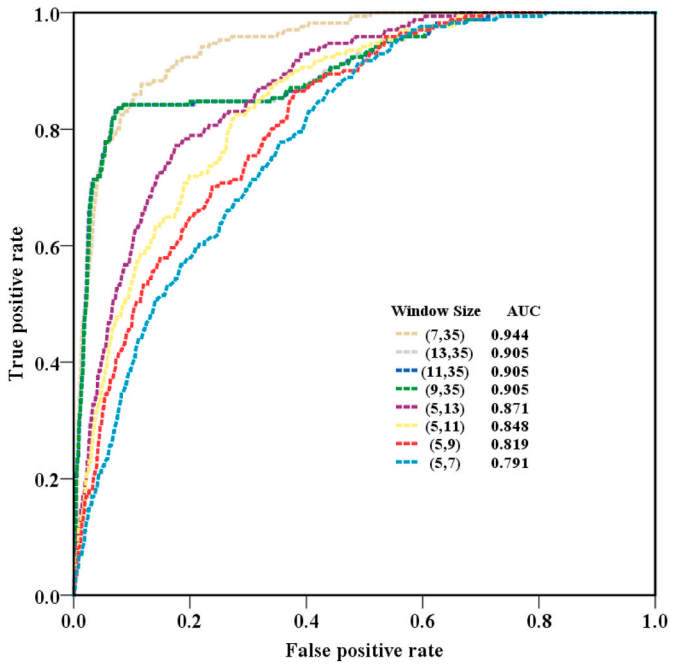

Fig. 9. AUC values of the obtained results using different dual-window sizes.

classification.

To train the CNN model, some parameters should be adjusted such as the learning rate, batch size, and window size. The learning rate determines the speed of back propagation, which can influence the training performance. According to the empirical studies, the CNN model achieved the best performance when the learning rate and batch size were set to 0.01 and 128, respectively.

During the training process, 10 random selected negative samples in non-mineralized areas were analyzed to verify whether the selection of negative samples influenced the training model and testing accuracy. Different selections of negative samples exhibited different losses and testing accuracies (Table 3). The fifth training dataset achieved the best training performance, with the training loss decreasing to 0.097 and the testing accuracy reaching 0.913 (Fig. 6).

4.3. Recognition of multivariate geochemical anomalies

The principle of identifying geochemical anomalies related to mineralization involves detecting deviations between the geochemical anomaly and the background. In the testing process, dual-window detection (Liu and Chang, 2013) was adapted for geochemical anomaly detection. Here, appropriate optimal window sizes need to be set based on the characteristics of the input geochemical exploration data. The CNN model can evaluate the difference between the selected pixels and surrounding pixels set by the inner and outer windows. Fig. 7 shows a sketch diagram with an internal window size of 3 × 3 and an outer window size of 5 × 5, resulting in 16 pixel pairs (i.e., {*T*, 1}, {*T*, 2}. . .{*T*, 16}). According to the principle of PPF, 16 values (dissimilarity = 0 or similarity = 1) were obtained. The average prediction value *D*(*T*) was calculated as the index of geochemical anomaly recognition. The CNN model generated corresponding prediction values of geochemical anomalies based on the differences between the inner and outer windows. The prediction values ranged from 0 to 1; the higher the prediction value, the higher the probability of a geochemical anomaly.

However, the size of the dual-window may affect the performance of geochemical anomaly detection. If the window size is extremely small, it may reflect a jump in the local value of elements. If the window size is very large, it may represent the geochemical background information. Therefore, experiments based on different window sizes were

conducted. To better compare the detection effect, geochemical anomaly maps were drawn based on the predicted values of different window sizes (Fig. 8). A cumulative probability of the results ranging from 0 to 5%, 5–15% and 15–30% indicated high (red), moderate (yellow), and low (blue) anomaly areas, respectively. Fig. 8 depicts the effects of window size on the mapping results.

The receiver operating characteristic (ROC) curve (Hanley and Mcneil, 1983) and the area under the ROC curve (AUC) have been widely applied to evaluate the performance of mineral prospectivity mapping and geochemical anomaly identification (e.g., Chen et al., 2014; Chen and Wu, 2017; Zuo, 2018). The AUC values (Fig. 9) indicated a good performance of the CNN based on pixel-pair matching. Moreover, the AUC values based on window sizes (13, 35) reached 0.905. The detected abnormal areas linked to high probability anomaly areas accounted for 5% of the total study area and contained almost 75% of the known Fe deposits. Thus, the obtained results were strongly spatially correlated with known Fe deposits. In addition, the areas linked to high probability were located in or near the contact zones of the C–P and Yanshanian intrusions, as well as the N-E faults, which are key controlling factors for the formation of Fe polymetallic mineralization in the study area (Fig. 8h) (Zhang and Zuo, 2014, 2015).

5. Conclusions

In this study, a hybrid method that combined the PPF method and a deep CNN was investigated with respect to multivariate geochemical anomaly identification in a case study in the southwest Fujian Province of China. The hybrid method was developed as follows: (i) a novel data augmentation algorithm (PPFs) was introduced to generate sufficient training samples to address the disadvantage of CNN which can be implemented only if the number of training samples is sufficient; and (ii) a deep CNN framework was constructed with optimum model parameters, e.g, the network depth, convolution layers, and window size, based on the generated sufficient training samples, to identify the multivariate geochemical anomalies associated with mineralization.

The identified geochemical anomalies exhibit a strong spatial correlation between the known locations of Fe polymetallic deposits and the predicted anomaly areas. Most of the known Fe deposits were located in high-probability areas, indicating that the proposed method is a powerful tool for identifying the multivariate geochemical anomalies associated with mineralization. In addition, this research provides a new approach for the application of supervised learning to other fields in geoscience to solve the lack of training samples.

Declaration of competing interest

The authors declare that they have no known competing financial interests or personal relationships that could have appeared to influence the work reported in this paper.

Acknowledgements

We thank two reviewers' comments and suggestions, which helped to improve this study. The research was supported by the National Natural Science Foundation of China (No. 41772344), MOST Special Fund from the State Key Laboratory of Geological Processes and Mineral Resources, China University of Geosciences (MSFGPMR03-3) and the Natural Resources Research Student Awards.

References

Aitchison, J., 1986. The Statistical Analysis of Compositional Data. Chapman & Hall, London, p. 416.
Anderson, J.A., 1972. A simple neural network generating an interactive memory. Math. Biosci. 14, 197–220.
Bergen, K.J., Johnson, P.A., De Hoop, M.V., Beroza, G.C., 2019. Machine learning for data-driven discovery in solid earth geoscience. Science 363 (6433) eaau0323.
Bezdek, J.C., Ehrlich, R., Full, W., 1984. FCM: the fuzzy c-means clustering algorithm. Comput. Geosci. 10, 191–203.
Bishop, C.M., 1995. Neural networks for pattern recognition. Agric. Eng. Int. CIGR J. 12, 1235–1242.
Breiman, L., 2001. Random forests. Mach. Learn. 45, 5–32.
Chen, Y., Lu, L., Li, X., 2014. Application of continuous restricted Boltzmann machine to identify multivariate geochemical anomaly. J. Geochem. Explor. 140, 56–63.
Chen, Y., Wu, W., 2017. Application of one-class support vector machine to quickly identify multivariate anomalies from geochemical exploration data. Geochem. Explor. Environ. Anal. 17, 231–238.
Chen, L., Guan, Q., Xiong, Y., Liang, J., Wang, Y., Xu, Y., 2019. A Spatially Constrained Multi-Autoencoder approach for multivariate geochemical anomaly recognition. Comput. Geosci. 125, 43–54.
Cheng, Q., 2007. Mapping singularities with stream sediment geochemical data for Prediction of undiscovered mineral deposits in Gejiu, Yunnan Province, China. Ore Geol. Rev. 32, 314–324.
Cheng, Q., 2012. Singularity theory and methods for mapping geochemical anomalies caused by buried sources and for predicting undiscovered mineral deposits in covered areas. J. Geochem. Explor. 122, 55–70.
Coates, A., Ng, A., Lee, H., 2011. An analysis of single-layer networks in unsupervised feature learning. In: Proceedings of the Fourteenth International Conference on Artificial Intelligence and Statistics, pp. 215–223.
Cohen, D.R., Kelley, D.L., Anand, R., Coker, W.B., 2010. Major advances in exploration geochemistry, 1998-2007. Geochem. Explor. Environ. Anal. 10, 3–16.
Cox, D.R., 1959. Corrigenda: the regression analysis of binary sequences. J. Roy. Stat. Soc. 21, 238.
Cracknell, M.J., Reading, A.M., 2013. The upside of uncertainty: identification of lithology contact zones from airborne geophysics and satellite data using random forests and support vector machines. Geophysics 78, WB113–WB126.
Dietterich, T.G., 2002. Ensemble learning. In: The Handbook of Brain Theory and Neural Networks, 2, pp. 405–408.
Egozcue, J.J., Pawlowsky-Glahn, V., Mateu-Figueras, G., Barcelo-Vidal, C., 2003. Isometric logratio transformations for compositional data analysis. Math. Geol. 35, 279–300.
Fodor, I.K., 2002. A survey of dimension reduction techniques. Neoplasia 9 10–20.
Gonbadi, A.M., Tabatabaei, S.H., Carranza, E.J.M., 2015. Supervised geochemical anomaly detection by pattern recognition. J. Geochem. Explor. 157, 81–91.
Grunsky, E.C., 2010. The interpretation of geochemical survey data. Geochem. Explor. Environ. Anal. 10, 27–74.
Guo, Y., Liu, Y., Oerlemans, A., Lao, S., Wu, S., Lew, M.S., 2016. Deep learning for visual understanding: a review. Neurocomputing 187, 27–48.
Hagemann, S.G., Lisitsin, V.A., Huston, D.L., 2016. Mineral system analysis: Quo vadis. Ore Geol. Rev. 76, 504–522.
Hanley, J.A., Mcneil, B.J., 1983. A method of comparing the areas under receiver operating characteristic curves derived from the same cases. Radiology 148, 839–843.
Hinton, G.E., Osindero, S., Teh, Y.W., 2006. A fast learning algorithm for deep belief nets. Neural Comput. 18, 1527–1554.
Karpatne, A., Ebert-Uphoff, I., Ravela, S., Babaie, H.A., Kumar, V., 2018. Machine learning for the geosciences: challenges and opportunities. IEEE Trans. Knowl. Data Eng. 31, 1544–1554.
Kirkwood, C., Cave, K., Beamish, D., Grebby, S., Ferreira, A., 2016. A machine learning approach to geochemical mapping. J. Geochem. Explor. 167, 49–61.
Krizhevsky, A., Sutskever, I., Hinton, G.E., 2012. ImageNet classification with deep convolutional neural networks. In: Advances in Neural Information Processing Systems, vol. 25, pp. 1097–1105.
LeCun, Y., Bengio, Y., Hinton, G., 2015. Deep learning. Nature 521, 436.
LeCun, Y., Bottou, L., Bengio, Y., Haffner, P., 1998. Gradient-based learning applied to document recognition. Proc. IEEE 86, 2278–2324.
Li, H., Li, X., Yuan, F., Jowitt, S.M., Zhang, M., Zhou, J., Wu, B., 2020. Convolutional neural network and transfer learning based mineral prospectivity modeling for geochemical exploration of Au mineralization within the Guandian–Zhangbaling area, Anhui Province, China. Appl. Geochem. 122, 104747.
Li, T., Zuo, R., Xiong, Y., Peng, Y., 2021. Random-drop data augmentation of deep convolutional neural network for mineral prospectivity mapping. Nat. Resour. Res. 30, 27–38.
Li, W., Wu, G., Zhang, F., Du, Q., 2016. Hyperspectral image classification using deep pixel-pair features. IEEE Trans. Geosci. Rem. Sens. 55, 844–853.
Liu, W.M., Chang, C.I., 2013. Multiple-window anomaly detection for hyperspectral imagery. IEEE J. Sel. Top. Appl. Earth Obs. Remote Sens. 6, 644–658.
Luo, Z., Xiong, Y., Zuo, R., 2020. Recognition of geochemical anomalies using a deep variational autoencoder network. Appl. Geochem. 122, 104710.
Mohri, M., Rostamizadeh, A., Talwalkar, A., 2018. Foundations of Machine Learning. MIT Press.
Redlich, A.N., 1993. Redundancy reduction as a strategy for unsupervised learning. Neural Comput. 5, 289–304.
Reichstein, M., Camps-Valls, G., Stevens, B., Jung, M., Denzler, J., Carvalhais, N., 2019. Deep learning and process understanding for data-driven earth system science. Nature 566 (7743), 195.
Scott, A.J., Knott, M., 1974. A cluster analysis method for grouping means in the analysis of variance. Biometrics 20, 507–512.
Shepard, D., 1968. A two-dimensional interpolation function for irregularly-spaced data. In: ACM National Conference, pp. 517–524.
Silverman, B.W., 1986. Density Estimation for Statistics and Data Analysis, vol. 175. Chapman & Hall, p. 12.

Singer, D.A., Kouda, R., 2001. Some simple guides to finding useful information in exploration geochemical data. Nat. Resour. Res. 10, 137–147.
Vapnik, V., 1995. The Nature of Statistical Learning Theory. Springer-Verlag, New York.
Wang, Z., Zuo, R., Dong, Y., 2019a. Mapping geochemical anomalies through integrating random forest and metric learning methods. Nat. Resour. Res. 28, 1285–1298.
Wang, Z., Dong, Y., Zuo, R., 2019b. Mapping geochemical anomalies related to Fe–polymetallic mineralization using the maximum margin metric learning method. Ore Geol. Rev. 107, 258–265.
Wang, J., Zuo, R., Xiong, Y., 2020. Mapping mineral prospectivity via semi–supervised random forest. Nat. Resour. Res. 29, 189–202.
Xie, X., Mu, X., Ren, T., 1997. Geochemical mapping in China. J. Geochem. Explor. 60, 99–113.
Xiong, Y., Zuo, R., 2016. Recognition of geochemical anomalies using a deep autoencoder network. Comput. Geosci. 86, 75–82.
Xiong, Y., Zuo, R., 2020. Recognizing multivariate geochemical anomalies for mineral exploration by combining deep learning and one-class support vector machine. Comput. Geosci. 140, 104484.
Xiong, Y., Zuo, R., 2021. Robust feature extraction for geochemical anomaly recognition using a stacked convolutional denoising autoencoder. Math. Geosci. https://doi.org/10.1007/s11004-021-09935-z.
Yousefi, M., Kreuzer, O.P., Nyknen, V., Hronsky, J.M.A., 2019. Exploration information systems - a proposal for the future use of GIS in mineral exploration targeting. Ore Geol. Rev. 111, 103005.
Yu, X., Xiao, F., Zhou, Y., Wang, Y., Wang, K., 2019. Application of hierarchical clustering, singularity mapping, and Kohonen neural network to identify Ag-Au-Pb-Zn polymetallic mineralization associated geochemical anomaly in Pangxidong district. J. Geochem. Explor. 203, 87–95.
Zhang, Z., Zuo, R., Cheng, Q., 2015a. The mineralization age of the Makeng Fe deposit, South China: implications from U-Pb and Sm-Nd geochronology. Int. J. Earth Sci. 104, 663–682.
Zhang, Z., Zuo, R., 2014. Sr–Nd–Pb isotope systematics of magnetite: implications for the genesis of Makeng Fe deposit, southern China. Ore Geol. Rev. 57, 53–60.
Zhang, Z., Zuo, R., Cheng, Q., 2015b. Geological features and formation processes of the Makeng Fe deposit, China. Resour. Geol. 65, 266–284.
Zhu, L., Chen, Y., Ghamisi, P., Benediktsson, J.A., 2018. Generative adversarial networks for hyperspectral image classification. IEEE Trans. Geosci. Rem. Sens. 56, 5046–5063.
Ziaii, M., Ardejani, F.D., Ziaei, M., Soleymani, A.A., 2012. Neuro-fuzzy modeling based genetic algorithms for identification of geochemical anomalies in mining geochemistry. Appl. Geochem. 27, 663–676.
Ziaii, M., Pouyan, A.A., Ziaei, M., 2009. Neuro-fuzzy modelling in mining geochemistry: identification of geochemical anomalies. J. Geochem. Explor. 100, 25–36.
Zuo, R., 2017. Machine learning of mineralization-related geochemical anomalies: a review of potential methods. Nat. Resour. Res. 26, 457–464.
Zuo, R., 2018. Selection of an elemental association related to mineralization using spatial analysis. J. Geochem. Explor. 184, 150–157.
Zuo, R., 2020. Geodata science-based mineral prospectivity mapping: a review. Nat. Resour. Res. 29, 3415–3424.
Zuo, R., Wang, J., 2016. Fractal/multifractal modeling of geochemical data: a review. J. Geochem. Explor. 164, 33–41.
Zuo, R., Xiong, Y., 2018. Big data analytics of identifying geochemical anomalies supported by machine learning methods. Nat. Resour. Res. 27, 5–13.
Zuo, R., Xiong, Y., 2020. Geodata science and geochemical mapping. J. Geochem. Explor. 209, 106431.
Zuo, R., Xiong, Y., Wang, J., Carranza, E.J.M., 2019. Deep learning and its application in geochemical mapping. Earth Sci. Rev. 192, 1–14.
Zuo, R., Zhang, Z., Zhang, D., Carranza, E.J.M., Wang, H., 2015. Evaluation of uncertainty in mineral prospectivity mapping due to missing evidence: a case study with skarn-type Fe deposits in Southwestern Fujian Province, China. Ore Geol. Rev. 71, 502–515.